Chemical Science

ROYAL SOCIETY OF CHEMISTRY

EDGE ARTICLE

View Article Online
View Journal | View Issue

Cite this: *Chem. Sci.*, 2021, **12**, 10063

All publication charges for this article have been paid for by the Royal Society of Chemistry

A crosslinked colloidal network of peptide/nucleic base amphiphiles for targeted cancer cell encapsulation†

Yanzi Zhou,[a] Peng Qiu,[a] Defan Yao,*[b] Yanyan Song,[a] Yuedong Zhu,[a] Haiting Pan,[a] Junchen Wu*[a] and Junji Zhang *[a]

Received 3rd June 2021
Accepted 22nd June 2021

DOI: 10.1039/d1sc02995a

rsc.li/chemical-science

The use of peptide amphiphiles (PAs) is becoming increasingly popular, not only because of their unique self-assembly properties but also due to the versatility of designs, allowing biological responsiveness, biocompatibility, and easy synthesis, which could potentially contribute to new drug design and disease treatment concepts. Oligonucleotides, another major functional bio-macromolecule class, have been introduced recently as new functional building blocks into PAs, further enriching the tools available for the fabrication of bio-functional PAs. Taking advantage of this, in the present work, two nucleic base-linked (adenine, A and thymine, T) RGD-rich peptide amphiphiles (NPAs) containing the fluorophores naphthalimide and rhodamine (**Nph-A** and **Rh-T**) were designed and synthesized. The two NPAs exhibit distinctive assembly behaviours with spherical (**Rh-T**) and fibrous (**Nph-A**) morphologies, and mixing **Nph-A** with **Rh-T** leads to a densely crosslinked colloidal network (**Nph-A**/**Rh-T**) *via* mutually promoted supramolecular polymerization *via* nucleation-growth assembly. Because of the RGD-rich sequences in the crosslinked network, further research on *in situ* targeted cancer cell (MDA-MB-231) encapsulation *via* RGD–integrin recognition was performed, and the modulation of cell behaviours (*e.g.*, cell viability and migration) was demonstrated using both confocal laser scanning microscopy (CLSM) imaging and a scratch wound healing assay.

Introduction

Peptide amphiphiles (PAs) are remarkably versatile and useful as building blocks for the construction of complex supramolecular structures using a bottom-up model.[1] To date, diversified supramolecular assembly strategies have been reported[2] and proven to be promising and powerful methods for biomedical materials with applications as antimicrobial agents,[3] in cancer therapy,[4] and in regenerative medicine.[5] Among the available assembly methods, the nucleation-growth mechanism is considered as one of the most promising strategies, because it allows the control of the self-assembly shape and the function of the peptides. In 2012, two PAs were designed to explore the growth mechanism of peptide amphiphiles in the presence of early formed spherical micelles.[6] More recently, Cui *et al.* took advantage of a small hydrophobic molecule, paclitaxel (PTX), as an effective promoter to induce nanofibre formation and elongation of a peptide–PTX conjugate.[7] Based on this mechanism, many attempts have been made to design stimuli-responsive peptide sequences and expand the scope of PA self-assembly in bio-applications. For example, peptides can be modified with enzyme-activated substrates that can perform spontaneous intracellular self-assembly upon interaction with specific enzymes, thus leading to cyto- or organelle-dysfunction.[8,9] This *in situ* nanodrug preparation strategy is now widely used as an efficient, targeted theranostic approach for cancer cells,[10,11] and can be applied to other tumour-related stimuli like microenvironments (*e.g.*, hypoxia, pH)[12,13] and small molecule metabolites (*e.g.*, ATP).[14] Moreover, the enzyme-activated intracellular colloidal formation can also act as a "nanoreactor" to facilitate *in situ* drug release and overcome the obstacle of inefficient dosing due to the relatively low concentration of drug uptake.[15]

Recently, nucleic bases have been introduced as new functional building blocks into the PAs,[16] due to their diverse stimuli-responsiveness (*e.g.*, high affinity with oligonucleotides,[17] multiple hydrogen bonding in duplexes/triplexes,[18] metal ion coordination,[19] pH/photo-responsiveness[20]) as well as good biocompatibility and biodegradability.[21] The design and

[a]*Key Laboratory for Advanced Materials and Joint International Research Laboratory of Precision Chemistry and Molecular Engineering, Feringa Nobel Prize Scientist Joint Research Center, School of Chemistry and Molecular Engineering, East China University of Science & Technology, 130 Meilong Road, Shanghai, 200237, China. E-mail: jcwu@ecust.edu.cn; zhangjunji@ecust.edu.cn*

[b]*Department of Radiology, Xinhua Hospital, Shanghai Jiao Tong University School of Medicine, 1665 Kongjiang Road, Shanghai, 200092, China. E-mail: yaodefan@xinhuamed.com.cn*

† Electronic supplementary information (ESI) available. See DOI: 10.1039/d1sc02995a

fabrication of nucleic based tethered PAs are thus enriched. Inspired by this, herein two nucleic base-linked (adenine, A and thymine, T) peptide amphiphiles (NPAs) containing the integrin-targeted RGD sequences were designed and synthesized (Fig. 1a). The two NPAs self-assemble into either spherical or fibrous nanostructures, whereas the mixture of these two NPAs (1 : 1) leads to a distinctive, mutually promoted supramolecular polymerization by a nucleation-growth assembly, resulting in the formation of a well-structured, densely crosslinked colloidal network. Taking advantages of the crosslinking peptide network and the integrin-targeted feature of the RGD sequences, an *in situ* "bottom-up" encapsulation of the targeted cancer cells (*e.g.*, MDA-MB-231, a triple negative breast cancer cell line that overexpresses integrin receptors) upon easy mixing of NPAs is achieved in this work (Fig. 1b). Different from the previously mentioned intracellular self-assembly approach, the NPA "capsule" directly interacts with receptors on the targeted MDA-MB-231 cytomembrane and may disturb the cellular mass and signal exchanges (*e.g.*, nutrient, metabolite or waste) between the cell and the surrounding micro-environment, thus imposing a negative effect on the cell stability and activity.[22] As a result, the viability and migration capability of the MDA-MB-231 cell line used are significantly affected by the crosslinked NPAs co-assembled on the cytomembrane, and thus, providing a new strategy for targeted cancer therapy.

Results and discussion

Molecular design

The two NPAs, adenine–RGDFFK–Nph (**Nph-A**) and thymine–RGDFFK–Rh (**Rh-T**), were designed and contained three regions. Region 1 is the nucleic base (A or T), which can enhance the intermolecular interactions with the help of hydrogen bonding. Region 2 is a short peptide (RGDFF), of which the RGD sequence is expected to increase the uptake of the peptides by the cancer cells *via* a mutual recognition mechanism with the integrin receptor. The diphenylalanine peptide (L-Phe-L-Phe, FF) is generally considered as the simplest peptide building block for self-assembly, and which has been demonstrated to self-assemble into well-ordered tubular structures with a long persistence length (~100 μm) by a combination of hydrogen bonding and π–π stacking of the aromatic residues.[23] Region 3 is the fluorophore of naphthalimide or rhodamine (Nph/Rh) with the lysine (K) link. The different geometry and π–π stacking interactions of the fluorophores together with the hydrogen-bonding of the peptide sequence FF determine the self-assembly types of the peptide amphiphiles **Nph-A** and **Rh-T** (Fig. 1a and S1–S3, ESI†).[24] According to the reported general procedure, both peptides, **Nph-A** and **Rh-T**, were synthesized using a manual Fmoc solid-phase peptide synthesis (SPPS) method, and were isolated by preparative HPLC on a reversed-phase C18 column with a 98.3%, and 98.5% purity and a 19.8%, and 20.6% in yield, respectively. The structures of both compounds were confirmed by analytical HPLC and mass spectrometry (Fig. S4–S6, ESI†).

Self-assembly of Nph-A and Rh-T

To investigate the self-assembly behaviour of the designed NPAs, **Nph-A** and **Rh-T** were all pre-treated in hexafluoroisopropanol (HFIP) to eliminate any pre-existing aggregates.[25] All HFIP treated samples were vacuum dried using a rotary evaporator, followed by addition of a Tris buffered saline buffer solution (TBS) to promote the formation of

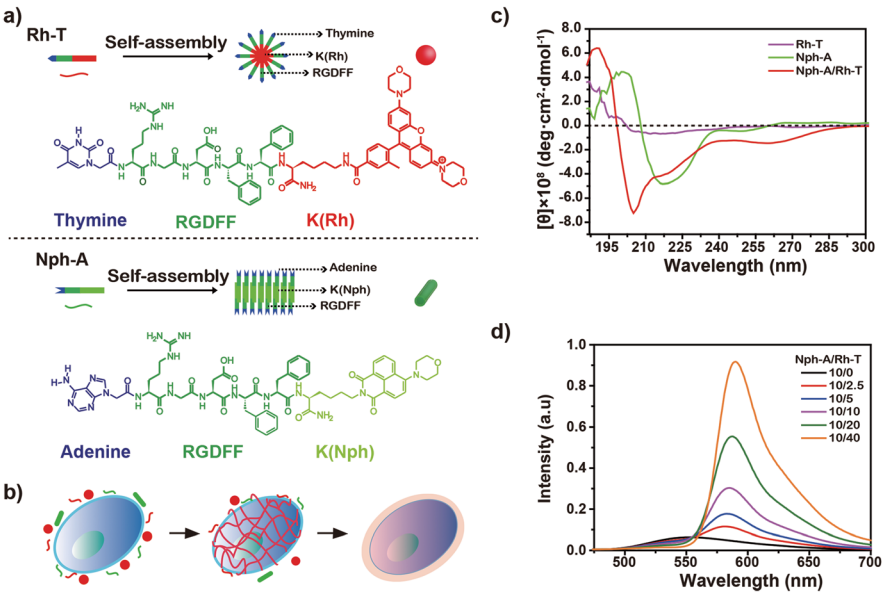

Fig. 1 (a) The molecular structures of peptides **Rh-T** and **Nph-A** and an illustration of the assembly of the peptides. (b) An illustration of cell encapsulation using the crosslinked **Nph-A**/**Rh-T** colloidal network on the cytomembrane. (c) Circular dichroism (CD) spectra of **Nph-A** (10.0 μM), **Rh-T** (10.0 μM), and **Nph-A**/**Rh-T** (10 μM, 1 : 1). (d) Fluorescence spectra of **Nph-A**/**Rh-T** formed with different ratios of **Nph-A** and **Rh-T** in TBS (50 mM Tris, pH 7.4, 25 °C).

discrete nanostructures. After 2 h of incubation, all the assembled nanostructures were imaged by transmission electron microscopy (TEM) to characterize their morphologies and dimensions. As shown in Fig. S7a (ESI†), **Nph-A** revealed a fibrous structure with uniform diameters of 10–15 nm (Fig. S8a, ESI†) and lengths reaching the micrometer-scale. In contrast, peptide **Rh-T** showed a spherical shaped aggregation with diameters of 20–40 nm (Fig. S7b and S8b, ESI†). The self-assembly behaviours of the peptides were further examined by dynamic light scattering (DLS, Fig. S9a, ESI†). The **Nph-A** and **Rh-T** formed different sized aggregations with diameters of 426 nm and 58 nm in a monomodal size distribution in TBS (50 mM Tris, pH 7.4, 25 °C), respectively. The differences in diameters and assembly structures might be due to the different hydrophobic groups/fluorophores (Region 3) linked to the peptide sequences. According to a molecular simulation study by Velichko[26] and Manandhar,[27] the assembly of a classic β-sheet-containing peptide amphiphile in aqueous solution can undergo two distinct pathways for the formation of supramolecular polymers, depending on the strength of hydrogen bonding relative to the interactions between the hydrophobic units. In the regime where hydrophobic interactions dominate, micellar aggregates are first formed, followed by the formation of hydrogen bonding in the periphery that eventually results in supramolecular polymeric growth. Thus, the extended π system and rigid planar structures of the 1,8-naphthalimide derivatives were beneficial to forming a co-facial structure, which leads to the nanostructure of the nanofibers. However, rhodamine's nonplanar configuration resulted in a different assembly morphology of the nanosphere.[28]

The secondary structures of the **Nph-A** and **Rh-T** assemblies were further characterized using circular dichroism (CD) and Fourier transform infrared (FTIR) spectroscopies. The CD spectrum of **Nph-A** showed a maximum peak at 200 nm and a minimum peak at 217 nm in TBS, which was characteristic of the formation of a twisted β-sheet structure (Fig. 1c).[29,30] Whereas the spherical **Rh-T** assembly did not display characteristic signals on the CD spectra, indicating its isotropic feature. The FTIR spectrum of **Nph-A** showed a strong band at 1637 cm^{-1} and a weak signal at 1550–1600 cm^{-1}, which are typical signals of an antiparallel β-sheet.[31] In contrast, **Rh-T** showed a broad peak at 1647 cm^{-1}, which is due to amide I absorption and the sharp peak at 1200–1250 cm^{-1} indicated a randomly coiled structure (Fig. S9b, ESI†).[32]

Crosslinking of Nph-A and Rh-T

Although individual **Nph-A** self-assembles into nanofibers and **Rh-T** self-assembles into spherical form, interestingly, the equivalent mixture of **Nph-A** and **Rh-T** (10 μM for each) unexpectedly led to a formation of a crosslinked fibril network with a uniform diameter of 8 nm and lengths reaching the micrometer-scale (Fig. S7c and S8c, ESI†). The DLS results showed a higher degree of NPA aggregation after the mixing of **Nph-A** and **Rh-T**. A double-modal size distribution appeared, which was consistent with the TEM results, indicating a possible crosslinking between **Nph-A** and **Rh-T** (Fig. S9a, ESI†). From the CD spectra, it can be assumed that the mixture assembled into highly oriented chiral structures *via* a stronger β-sheet formation that led to both an increased positive peak at 190 nm and a negative peak at 205 nm. The negative peak at 218 nm could be attributed to the π–π stacking of the aromatic side chains FF and to the distortion of the β-sheets, which was also much stronger than the **Nph-A** assembly alone (Fig. 1c).[33] A weak peak at around 260–280 nm revealed the existence of the helical stacking of adenine and thymine. Fluorescence emission spectroscopy was also performed to check the Förster resonance energy transfer (FRET) between the naphthalimide in **Nph-A** and the rhodamine in **Rh-T**. The **Nph-A** and **Rh-T** showed remarkable fluorescence at 527 nm and 589 nm in TBS, respectively. The fluorescence intensity of the **Nph-A**/**Rh-T** mixture (from 4 : 1 to 1 : 4) showed a decrease at 527 nm and a subsequent increase at 589 nm (Fig. 1d), which demonstrated the efficient FRET between the naphthalimide in **Nph-A** and the rhodamine in **Rh-T**. This result provides more evidence for the crosslinking of **Nph-A** and **Rh-T** because the efficient FRET can be attributed to the shortened distance between the two fluorophores. The freeze-dried **Nph-A**/**Rh-T** were also characterized by scanning electron microscopy (SEM) and porous microstructures were observed, a typical hydrogel-like structure previously reported for other supramolecular hydrogels (Fig. S10, ESI†),[34,35] demonstrating again the crosslinking feature of **Nph-A**/**Rh-T**.

It was speculated that the peptide self-assembly as well as hydrogen bonding from the nucleic bases might induce the crosslinking of **Nph-A**/**Rh-T**. The two aromatic peptides were blended to form a hydrophobic area, together with phenylalanine. At the same time, adenine and thymine formed an additional hydrogen bonding based on the complementary pairing, further strengthening the crosslinking between the peptide monomers. As previously reported, Shimada *et al.* observed the formation of spherical micelles as a precursor morphology prior to their elongation into long filamentous structures.[36] In this research, it is hypothesized that the crosslinking was promoted by enhanced hydrogen binding between two NPAs. The assembled **Rh-T** spherical micelles as the precursor morphology promoted the extension of the assembled **Nph-A**, which lead to the formation of the fiber network.

In order to investigate the role of nucleic bases in supramolecular self-assembly, a control peptide was further synthesized with thymine replacing adenine as **Nph-T** (Fig. S3, ESI†). The TEM image shows that **Nph-T** itself forms nanofibers with diameters of 14–16 nm and lengths in the micron range, similar to that of **Nph-A** (Fig. S7d, ESI†). Yet, no crosslinked network was observed when mixing **Nph-T** with **Rh-T** (molar ratio of 1 : 1, 10 μM, Fig. S7e, ESI†). To determine the optimized assembly ratio, a series of **Nph-A**/**Rh-T** mixtures with ratios of 4 : 1 to 1 : 2 were prepared (aged for 2 h) for examining the crosslinking performances of these two NPAs. At all ratios, the TEM images exhibited a long fiber network with diameters of *ca.* 6–8 nm. As the amount of **Rh-T** increased, the density of the fiber network increased and a densely crosslinked fiber network was observed when the ratio was increased to 1 : 1 (Fig. 2a–d). The morphology and network density did not vary obviously

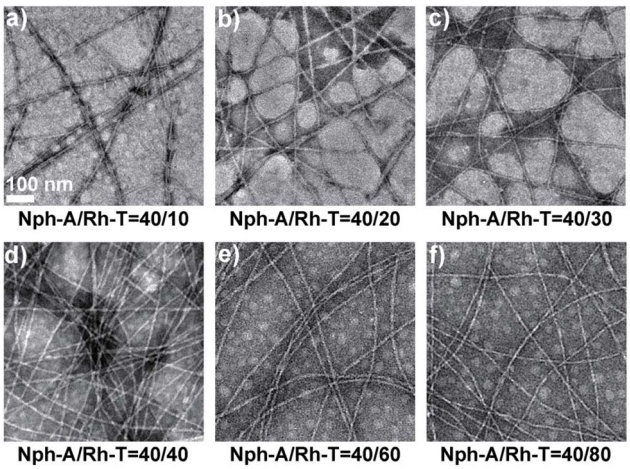

Fig. 2 Transmission electron microscopy (TEM) images of the assemblies of mixtures with different molar ratios of **Nph-A**/**Rh-T**: (a) 4 : 1, (b) 2 : 1, (c) 4 : 3, (d) 1 : 1, (e) 2 : 3, and (f) 1 : 2 (**Nph-A** = 10 μM). Scale bar = 100 nm.

when the amount of **Rh-T** was further increased (Fig. 2e and f). Therefore, an equal ratio of the **Nph-A**/**Rh-T** mixture was selected for further applications in *in situ* cell encapsulation.

Cellular uptake and encapsulation

As an important member of the integrin family, the adhesion molecule αvβ3 has been widely investigated for use in tumour imaging and therapy because of its pivotal roles in tumour proliferation and metastasis. In particular, due to its upregulated expression in proliferating tumour cells compared to normal cells with a low αvβ3 expression, integrin αvβ3 has been identified as an ideal therapeutic target for tumour therapy. The peptide ligands containing the RGD motif, which shows a strong binding affinity and selectivity to integrin αvβ3, have been employed as tumour-homing ligands for integrin targeted therapeutic applications.

In this work, it was assumed that the densely crosslinked network of **Nph-A**/**Rh-T** together with the RGD-rich feature might form a peptide "cocoon" that encapsulated the αvβ3-overexpressed tumour cells. To verify the hypothesis, the *in situ* cell encapsulation performances of the **Nph-A**/**Rh-T** network were investigated by confocal laser scanning microscopy (CLSM) after incubation with two cell lines of MDA-MB-231 (human breast cancer cell that overexpress the integrin αvβ3 (ref. 37)) and HeLa (human cervical carcinoma that has limited integrin αvβ3 expression[38]). After incubation with RGD-rich **Rh-T** for 2.5 h, both αvβ3-positive MDA-MB-231 cells and αvβ3-negative HeLa cell lines exhibited a red fluorescence in cytoplasm, which was probably due to the internationalization of the nanoparticle-sized **Rh-T** assembly through the lysosomal pathway (Fig. S11a–d and S12a–d, ESI†).[39] Both cell lines treated with **Nph-A** showed a negligible green fluorescence, which might be attributed to the fibrous morphology of **Nph-A** that was unfavorable for cell uptake (Fig. S11e–h and S12e–h, ESI†).

Interestingly, the MDA-MB-231 cells incubated with **Nph-A**/**Rh-T** exhibited an obviously enhanced red fluorescence of rhodamine along the outline of the cells rather than in the cytoplasm (Fig. S11i–l, ESI†), when compared with use of **Rh-T** alone. This might indicate the possible interactions between the overexpressed integrin αvβ3 on the cytomembrane of MDA-MB-231 cells and the RGD-rich **Nph-A**/**Rh-T** networks that lead to their encapsulation on the cell surface. Conversely, no obvious sign of cell encapsulation was detected in HeLa cells, as the red rhodamine fluorescence was mainly observed in the cytoplasm (Fig. S12i–l, ESI†), similar to the case shown in Fig. S12a–d (ESI†). The sharp difference of the encapsulation performance on HeLa cells might be attributed to the limited expression of the integrin αvβ3 receptor on the HeLa cell membrane.

To further identify the **Nph-A**/**Rh-T** network with RGD sequence formed encapsulation on the cell surface of the MDA-MB-231 cells, the cytomembrane was stained with DiD ($DiIC_{18}(5)$, Biotium), a commercially available membrane-staining dye, and performed the colocalization imaging of the co-stained cell surface (Fig. 3 and S13, ESI†). As shown in Fig. 3e–h and S13e–h (ESI†), the cells treated with **Nph-A**/**Rh-T** exhibited red rhodamine fluorescence that overlapped well with the fluorescence of the cytomembrane stain DiD, indicating the formation of crosslinked peptide capsules on the cell surface. Conversely, colocalization of fluorescence between rhodamine and DiD was not observed when the cells were incubated with **Rh-T** alone (Fig. 3a–d and S13a–d, ESI†) or non-crosslinked

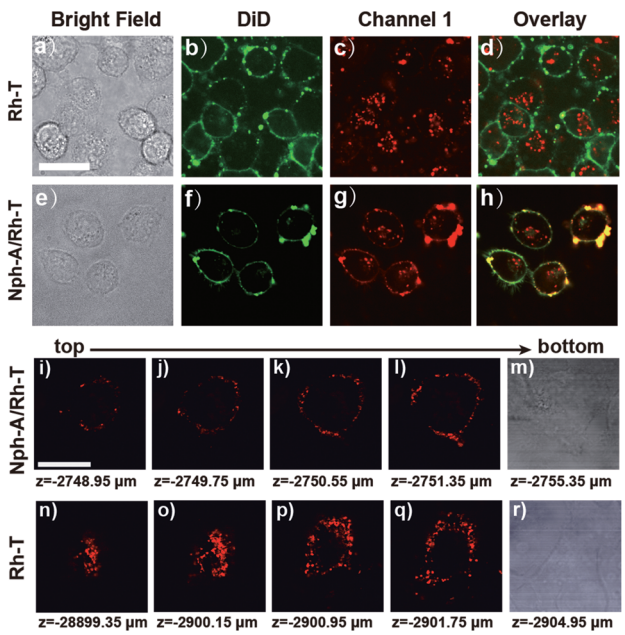

Fig. 3 Confocal fluorescence images of (a–d) MDA-MB-231 cells incubated with **Rh-T** (10 μM) and stained with DiD (20 μM); and (e–h) MDA-MB-231 cells incubated with **Nph-A**/**Rh-T** (1 : 1, **Nph-A** = 10 μM and **Rh-T** = 10 μM) and stained with DiD (20 μM). 3D confocal images of channel 1 (red) of the MDA-MB-231 cells incubated with (i–m) **Nph-A**/**Rh-T** (1 : 1, **Nph-A** = 10 μM and **Rh-T** = 10 μM) and (n–r) **Rh-T** (= 20 μM). Scanned from bottom to top. Channel DiD: excitation: 640 nm, emission collected: 663–738 nm. Channel 1 for **Rh-T**: excitation: 561 nm, emission collected: 570–620 nm. Scale bar: 10 μm.

Nph-T/**Rh-T** (Fig. S13i–l, ESI†), further proving the crucial role of the crosslinked **Nph-A**/**Rh-T** network on the efficient cell encapsulation.

Next, the 3D confocal imaging of MDA-MB-231 cell with **Nph-A**/**Rh-T** was performed. The bright red circle of fluorescence, whose diameter gradually shrank when the cell was scanned from bottom to top, showed the spatial encapsulation of the MDA-MB-231 cell (Fig. 3i–m). As a control experiment, cells were cultured with **Rh-T** alone (Fig. 3n–r) and a bright mass of red fluorescence with an unclear outline was observed instead. These results demonstrated that the **Nph-A**/**Rh-T** network was able to specifically attach onto the cell surface and it prevented itself from being endocytosed into the cytoplasm.

Cell viability and migration assays

To examine whether the cell encapsulation with the **Nph-A**/**Rh-T** network could affect the cell behaviours of αvβ3-positive MDA-MB-231, *e.g.*, viability and migration, the CCK-8 and scratch wound healing assays were investigated. Firstly, as revealed by the CCK-8 assay, the MDA-MB-231 cells cultured with **Rh-T** (0–50 μM) showed good viabilities of over 90% after 24 h incubation (Fig. 4a). The MDA-MB-231 cells cultured with **Nph-A** (0–50 μM) also showed good viability, although a little lower than that of **Rh-T** at high concentrations. This difference might be attributed to the potential cytotoxicity of the fibrous **Nph-A** assembly attached to the cytomembrane in high concentrations.[22] These results provide evidence that neither **Rh-T** or **Nph-A** would affect the cell viability. The crosslinked **Nph-A**/**Rh-T**, however, exhibited a significant impact on the viability of the MDA-MB-231 cells viability (45.6%) when reaching a concentration of 12.5 μM. It was assumed that the encapsulation of MDA-MB-231 cells *via* RGD-αvβ3 recognition of the crosslinking networks composed of **Nph-A**/**Rh-T** could hamper materials (nutrients and metabolites) and signal transportation between the cells and the surrounding micro-environment, which leads to the decreased cell viability. To further confirm that the RGD-αvβ3 recognition is responsible for the observed cell inhibition, the MDA-MB-231 cells were pre-treated with the αvβ3 inhibitor (cilengitide, Cil) before incubation with **Nph-A**/**Rh-T**. In sharp contrast, the cells successively treated with Cil and **Nph-A**/**Rh-T** showed limited cell inhibition even at a high **Nph-A**/**Rh-T** concentrations, indicating that the interaction between the αvβ3 and RGD-containing peptides facilitated the cell encapsulation by αvβ3 recognition (Fig. 4a). Moreover, control experiments were also performed on the HeLa cell line, which had limited αvβ3 expression. The CCK-8 assay exhibited similar cell viability (80–90%) upon treatment with **Rh-T**, **Nph-A** and **Nph-A**/**Rh-T**, in different concentrations (Fig. S14a, ESI†), indicating the negligible inhibition effects of the **Nph-A**/**Rh-T** crosslinked network on the HeLa cells, on account of inefficient encapsulation.

The inhibitory action on cell migration was further evaluated using a scratch wound healing assay. As shown in Fig. 4b, the scratched cell "wound" was photographed at 0 and 24 h before and after various treatments. It was clearly seen that the control

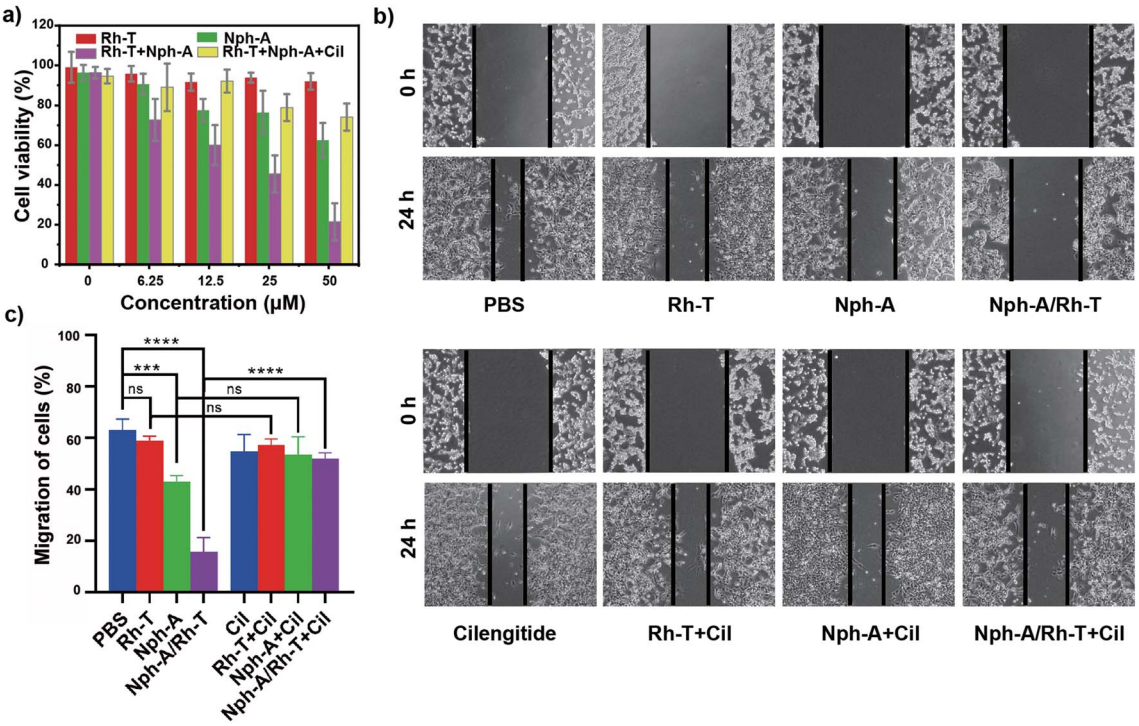

Fig. 4 (a) Results of the CCK-8 assay of MDA-MB-231 cells incubated with **Rh-T**, **Nph-A**, and **Nph-A**/**Rh-T** (1 : 1) at various concentrations (0 μM, 6.25 μM, 12.5 μM, 25 μM, and 50 μM). (b) Results of the scratch wound healing assays of MDA-MB-231 cells with **Rh-T** (12.5 μM), **Nph-A** (12.5 μM), and **Nph-A**/**Rh-T** (1 : 1, 12.5 μM) with and without cilengitide (Cil, 40 μM). (c) Quantification of the migration rates of cells (%). ns ≥ 0.05, ***p < 0.001, ****p < 0.0001.

MDA-MB-231 cells had a nearly healed "wound" after 24 h incubation, whereas the wound closure was inhibited by different amounts after **Rh-T**, **Nph-A** and **Nph-A/Rh-T** treatments for 24 h, and **Nph-A/Rh-T** showed the highest inhibition. However, pre-treatment of the cells by an αvβ3 inhibitor (cilengitide, Cil) before the treatments showed similar wound closures after 24 h, suggesting that αvβ3 recognition played a crucial role in cell migration. To quantify the inhibition of cell migration, the wound area was determined and the average migration rate of the cells was calculated.[40] As shown in Fig. 4c, the cell migration speed of the control group was 63.0%. After treatments for 24 h, the cell migration speed of the **Rh-T**, **Nph-A** and **Nph-A/Rh-T** groups decreased to 59.0%, 51.5%, and 15.7%, respectively, and the cells pre-treated with Cil showed no significant difference to the control cells. The same experiments were also carried out using HeLa cell lines (Fig. S14b and c, ESI†). As expected, no evident inhibitory effects were discovered when treating the HeLa cells with **Rh-T** (26.7%), **Nph-A** (26.6%) and **Nph-A/Rh-T** (27.6%) for 24 h, when compared to the control group (26.6%). These results demonstrated that the cell-encapsulation with a RGD-rich **Nph-A/Rh-T** network could inhibit the proliferation and migration of tumour cells *via* αvβ3 recognition.

Conclusions

In summary, two nucleic base-linked peptide amphiphiles (NPAs) that displayed different assembly performances were designed and synthesized. Peptide **Nph-A** with adenine as the N-terminal aggregates into a twisted ribbon structure due to β-sheet formation. Peptide **Rh-T** with thymine as the N-terminal induces isotropic molecular packing, resulting in spherical micelles. Interestingly, the crosslinking of **Nph-A** and **Rh-T** leads to the formation of a densely crosslinked colloidal network stabilized *via* hydrogen bonding between adenine and thymine. Taking advantage of the RGD-rich peptide crosslinked network, it was further applied to targeted cancer cell encapsulation *via* RGD–integrin recognition, and the manipulation of cell behaviours (*e.g.*, cell migration) was demonstrated. It is expected that this design strategy will provide a general approach for controlling/modulating the biological behaviours and processes of targeting cells *via* self-assembly-facilitated cell surface engineering, which could one day lead to diverse applications in cancer theranostics and single cell studies.

Data availability

Further details of the experiments are available in the ESI.

Author contributions

Y. Zhou, D. Yao and J. Zhang designed the study. Y. Zhou, D. Yao, P. Qiu performed the experiments. Y. Zhou, D. Yao and J. Zhang analyzed the data. Y. Song, Y. Zhu and H. Pan made contribution to the discussions during the work. Y. Zhou, D. Yao and J. Zhang prepared the manuscript. J. Wu and J. Zhang concepted the project and supervised this research. All authors provided feedback on the paper.

Conflicts of interest

There are no conflicts to declare.

Acknowledgements

The authors acknowledge financial support from the NSFC (21878086, 21788102) and the Shanghai Rising-Star Program (19QA1402500 to JZ). The project was supported by the Shanghai Municipal Science and Technology Major Project (Grant No. 2018SHZDZX03), the International Cooperation Program of Shanghai Science and Technology Committee (17520750100), and the Fundamental Research Funds for the Central Universities (222201717003).

References

1 V. Percec, G. Ungar and M. Peterca, *Science*, 2006, **313**, 55–56.
2 Z. F. He, W. Jiang and C. A. Schalley, *Chem. Soc. Rev.*, 2015, **44**, 779–789.
3 G. Laverty, A. P. McCloskey, B. F. Gilmore, D. S. Jones, J. Zhou and B. Xu, *Biomacromolecules*, 2014, **15**, 3429–3439.
4 Y. Kuang and B. Xu, *Angew. Chem., Int. Ed.*, 2013, **52**, 6944–6948.
5 B. Pena, V. Martinelli, M. Jeong, S. Bosi, R. Lapasin, M. R. G. Taylor, C. S. Long, R. Shandas, D. Park and L. Mestroni, *Biomacromolecules*, 2016, **17**, 1593–1601.
6 T. Shimada, N. Sakamoto, R. Motokawa, S. Koizumi and M. Tirrell, *J. Phys. Chem. B*, 2012, **116**, 240–243.
7 H. Su, W. J. Zhang, H. Wang, F. H. Wang and H. G. Cui, *J. Am. Chem. Soc.*, 2019, **141**, 11997–12004.
8 P. Chandra Saha, R. S. Das, T. Chatterjee, M. Bhattacharyya and S. Guha, *Bioconjugate Chem.*, 2020, **31**, 1301–1306.
9 M. T. Jeena, L. Palanikumar, E. M. Go, I. Kim, M. G. Kang, S. Lee, S. Park, H. Choi, C. Kim, S. M. Jin, S. C. Bae, H. W. Rhee, E. Lee, S. K. Kwak and J. H. Ryu, *Nat. Commun.*, 2017, **8**, 26.
10 W. Du, X. Hu, W. Wei and G. Liang, *Bioconjugate Chem.*, 2018, **29**, 826–837.
11 Z. Feng, X. Han, H. Wang, T. Tang and B. Xu, *Chem*, 2019, **5**, 2442–2449.
12 J. Y. Li, K. J. Shi, Z. F. Sabet, W. J. Fu, H. Zhou, S. X. Xu, T. Liu, M. You, M. J. Cao, M. Z. Xu, X. J. Cui, B. Hu, Y. Liu and C. Y. Chen, *Sci. Adv.*, 2019, **5**, eaax0937.
13 M. Li, Y. Ning, J. Chen, X. Duan, N. Song, D. Ding, X. Su and Z. Yu, *Nano Lett.*, 2019, **19**, 7965–7976.
14 H. Wang, Z. Feng, Y. Qin, J. Wang and B. Xu, *Angew. Chem., Int. Ed.*, 2018, **57**, 4931–4935.
15 H. W. An, L. L. Li, Y. Wang, Z. Wang, D. Hou, Y. X. Lin, S. L. Qiao, M. D. Wang, C. Yang, Y. Cong, Y. Ma, X. X. Zhao, Q. Cai, W. T. Chen, C. Q. Lu, W. Xu, H. Wang and Y. Zhao, *Nat. Commun.*, 2019, **10**, 4861.
16 R. Patel, S. Sarma, A. Shukla, P. Parmar, D. Goswami and M. Saraf, *Mol. Biol. Rep.*, 2020, **47**, 8113–8131.

17 M. O. Guler, J. K. Pokorski, D. H. Appella and S. I. Stupp, *Bioconjugate Chem.*, 2005, **16**, 501–503.
18 G. T. Brinke, L. Bouteiller, O. Ikkala and W. Binder, *Hydrogen Bonded Polymers*, Springer-Verlag, Berlin, 2007, vol. 207, pp. 113–177.
19 Y. Y. Lin, E. T. Pashuck, M. R. Thomas, N. Amdursky, S. T. Wang, L. W. Chow and M. M. Stevens, *Angew. Chem., Int. Ed.*, 2017, **56**, 2361–2365.
20 O. Berger, L. Adler-Abramovich, M. Levy-Sakin, A. Grunwald, Y. Liebes-Peer, M. Bachar, L. Buzhansky, E. Mossou, V. T. Forsyth, T. Schwartz, Y. Ebenstein, F. Frolow, L. J. Shimon, F. Patolsky and E. Gazit, *Nat. Nanotechnol.*, 2015, **10**, 353–360.
21 D. Yuan, X. W. Du, J. F. Shi, N. Zhou, J. Zhou and B. Xu, *Angew. Chem., Int. Ed.*, 2015, **54**, 5705–5708.
22 Y. Kuang, J. F. Shi, J. Li, D. Yuan, K. A. Alberti, Q. B. Xu and B. Xu, *Angew. Chem., Int. Ed.*, 2014, **53**, 8104–8107.
23 X. H. Yan, P. L. Zhu and J. B. Li, *Chem. Soc. Rev.*, 2010, **39**, 1877–1890.
24 M.-Y. Yeh, C.-T. Huang, T.-S. Lai, F.-Y. Che, N.-T. Chu, D. T.-H. Tseng, S.-C. Hung and H.-C. Lin, *Langmuir*, 2016, **32**, 7630–7638.
25 M. Kumar, N. Kumar, V. Bhalla, H. Singh, P. R. Sharma and T. Kaur, *Org. Lett.*, 2011, **13**, 1422–1425.
26 Y. S. Velichko, S. I. Stupp and M. O. de la Cruz, *J. Phys. Chem. B*, 2008, **112**, 2326–2334.
27 A. Manandhar, M. Kang, K. Chakraborty, P. K. Tang and S. M. Loverde, *Org. Biomol. Chem.*, 2017, **15**, 7993–8005.
28 F. L. Arbeloa, P. R. Ojeda and I. L. Arbeloa, *J. Lumin.*, 1989, **44**, 105–112.
29 C. Lara, N. P. Reynolds, J. T. Berryman, A. Q. Xu, A. F. Zhang and R. Mezzenga, *J. Am. Chem. Soc.*, 2014, **136**, 4732–4739.
30 B. Ranjbar and P. Gill, *Chem. Biol. Drug Des.*, 2009, **74**, 101–120.
31 J. Bandekar and S. Krimm, *Biopolymers*, 1988, **27**, 909–921.
32 Y. A. Lazarev, B. A. Grishkovsky and T. B. Khromova, *Biopolymers*, 1985, **24**, 1449–1478.
33 C. J. Bowerman, W. Liyanage, A. J. Federation and B. L. Nilsson, *Biomacromolecules*, 2011, **12**, 2735–2745.
34 Z. Y. Li, G. Davidson-Rozenfeld, M. Vázquez-González, M. Fadeev, J. J. Zhang, H. Tian and I. Willner, *J. Am. Chem. Soc.*, 2018, **140**, 17691–17701.
35 Z. Y. Li, Y. Y. Liu, Y. J. Li, W. H. Wang, Y. Y. Song, J. J. Zhang and H. Tian, *Angew. Chem., Int. Ed.*, 2021, **60**, 5157–5161.
36 T. Shimada, N. Sakamoto, R. Motokawa, S. Koizumi and M. Tirrell, *J. Phys. Chem. B*, 2012, **116**, 240–243.
37 Z. Liu, W. Chen, Y. H. Li and Q. Xu, *Anal. Chem.*, 2016, **88**, 11955–11962.
38 C. Bolzati, N. Salvarese, D. Carpanese, R. Seraglia, L. Melendez-Alafort, A. Rosato, D. Capasso, M. Saviano, A. Del Gatto, D. Comegna and L. Zaccaro, *J. Med. Chem.*, 2018, **61**, 9596–9610.
39 Q. Q. Hu, H. Li, L. H. Wang, H. Z. Gu and C. H. Fan, *Chem. Rev.*, 2019, **119**, 6459–6506.
40 A. Grada, M. Otero-Vinas, F. Prieto-Castrillo, Z. Obagi and V. Falanga, *J. Invest. Dermatol.*, 2017, **137**, e11–e16.